Rotating properties of Bragg reflections and spatial lattice solitons in rotating photonic lattices

Zaifei Song (宋载飞), Sheng Liu (刘 圣), Xuetao Gan (甘雪涛), Jianlin Zhao (赵建林)*, and Enpu Li (李恩普)

Shaanxi Key Laboratory of Optical Information Technology, The Key Laboratory of Space Applied Physics and Chemistry, Ministry of Education, School of Science, Northwestern Polytechnical University, Xi'an 710072, China

**Corresponding author: jlzhao@nwpu.edu.cn*

Received December 2, 2010; accepted January 28, 2011; posted online May 26, 2011

We demonstrate the rotating properties of Bragg reflections and spatial lattice solitons in rotating photonic lattices by analyzing the linear and nonlinear propagations of light. It reveals that the Bragg reflection of the light waves rotates synchronously with the lattices, leading to the rotation of the Bloch waves during propagations. In the presence of nonlinearity, rotating lattice solitons from different transmission bands can propagate in a relatively stable manner. However, reduced-symmetry solitons at point X_2 cannot easily rotate synchronously with the lattice, owing to Coriolis forces. Moreover, additional angular momenta are added to the off-axis propagating solitons.

OCIS codes: 080.1238, 190.4420.
doi: 10.3788/COL201109.070801.

In recent years, linear and nonlinear propagations of light in photonic lattices have attracted growing interest among researchers[1−15]. When a light wave propagates in a linear photonic lattice, it is modulated periodically in accordance with the Floquet-Bloch theorem. Due to the Bragg reflection of the periodic potential, the continuous spatial transmission spectrum is split into separate bands by the forbidden gaps at the boundaries of the Brillouin zone[1−3]. On the basis of the band-gap structures, intriguing phenomena have been demonstrated in the photonic lattices, such as discrete diffraction[1], anomalous diffraction and refraction[4−6], as well as Bloch waves[6−9]. In the presence of nonlinearity, discrete diffractions can be counteracted by the nonlinearity, before finally achieving stable localized states as lattice solitons[10−15]. Specifically, photonic lattices with a rotating property provide more interesting dynamics than their stationary counterparts. In addition, various fascinating phenomena have been demonstrated in rotating optical systems. For instance, in a twisted fiber, propagating light can acquire new polarization dynamics, and experience suppressed tunneling to an adjacent fiber[16,17]. In addition, the nonlinear light propagations in rotating waveguide arrays have been reported in a photorefractive crystal, where in-band and multi-band wave couplings and lattice solitons are experimentally observed under noninertial (centripetal and Coriolis) forces[18]. In a cold atom system, the rotating square potentials were introduced in Bose-Einstein condensates that supported stable fundamental and vortex solitons[19,20]. Resembling the case in curved lattices, the couplings of the underlying Bloch modes were modified in a rotating photonic lattice[21]. In this letter, the Bragg reflection in the rotating lattice is also changed rather than in the curved lattice. The rotating properties of the Bragg reflections and lattice solitons are demonstrated by analyzing the linear and nonlinear propagations of light in rotating photonic lattices. The Bloch waves and gap solitons with the rotation property are stimulated under tricky initial conditions. This reveals that the rotation of the Bragg reflection benefits the stability of the lattice solitons, which may also be affected by Coriolis forces.

The nonlinear propagation of a probe beam in a biased photorefractive crystal with rotating photonic lattices could be described by the dimensionless model initially deduced by Zozulya *et al.*[22]. When the characteristic spatial scale is larger than the photorefractive Debye length, and assuming the diffusion effect can be neglected, the steady-state propagations of the probe beam in the rotating photonic lattices are governed by

$$\left(\frac{\partial}{\partial_z} - \frac{\mathrm{i}}{2}\nabla_\perp^2\right)\mathbf{B} = \mathrm{i}\left(V_l + E_0\frac{|\mathbf{B}|^2}{1+|\mathbf{B}|^2}\right)\mathbf{B}, \quad (1)$$

where $\mathbf{B}$ is the complex amplitude of the probe beam, $\nabla_\perp^2 = \partial_{xx} + \partial_{yy}$, and E_0 is the external bias field. Here, the periodic potential of the rotating lattice V_l is described by

$$\begin{cases} V_l = V_0\cos^2(\pi x_1/d)\cos^2(\pi y_1/d) \\ x_1 = x\cos(\delta_\theta z) + y\sin(\delta_\theta z) \\ y_1 = -x\sin(\delta_\theta z) + y\cos(\delta_\theta z) \end{cases}, \quad (2)$$

where V_0 is the peak value of the lattice potential, d is the period, and δ_θ denotes the rotation velocity of the lattice along z-axis. A geometric schematic of the rotating photonic lattices is shown in Fig. 1(a), which shows that the lattice sites rotate around the z-axis, while the central site remains stationary.

Calculating the Brillouin zone spectra (BZSs) is essential in analyzing the Bragg reflections of the rotating photonic lattices. In the photonic lattice, the light components with spatial frequency near the Brillouim zone (BZ) boundaries are selectively reflected according to the Bragg's law; as a result, the corresponding regions in momentum space receive weak illumination and present dark lines[2,3]. These dark lines represent the BZ boundaries and the intensities of the corresponding Bragg reflections.

Here, we used the simulation parameters $\delta_\theta=\pi/600$, $d=5$, and $V_0=0.5$, and employed the method proposed in Ref. [3] to calculate the BZSs of the rotating lattices depicted in Eq. (2). Figure 1(b) is the BZSs of the stationary lattice, and Figs. 1(c) and (d) are the BZSs of the rotating lattice depicted in Eq. (2) at z=100 and 150, respectively. Unlike the stationary lattice, the BZSs did not remain stationary but revolved synchronously with the lattice, i.e., the BZSs and lattice revolved at the same angle of 30° (45°) at z=100 (150) (Figs. 1(c) and (d)). Considering that the propagation of light with the spectrum close to the BZ boundaries of the photonic lattice acted upon by the Bragg reflection, the "force" generated by the rotating Bragg reflection may drive light to turn around along with the lattice.

Meanwhile, we studied the propagation of the Bloch modes of high-symmetry points at the BZ boundaries, where they suffered from strong Bragg reflections. To excite the pure Bloch modes, the profiles of the input beams were modulated by the phase structures of corresponding Bloch waves (see the left panels of Figs. 2(b)−(e)), as previously reported in Ref. [7]. For the excitation of points X_1, M_1, X_2, and M_2, the input beams were constructed with the expressions of $\exp[-(x/12)^2-(y/12)^2]\cos(\pi x/5)$, $\exp[-(x/12)^2-(y/12)^2]\cos(\pi x/5)\cos(\pi y/5)$, $\exp[-(x/12)^2-(y/12)^2]\sin(\pi x/5)$, and $\exp[-(x/12)^2-(y/12)^2]\sin(\pi x+y)/5)$, respectively (insets of Figs. 2(b)−(e)). Taking the input beams constructed above as the initial conditions, the light propagations in the rotating photonic lattices were simulated by solving the linear version ($E_0=0$) of Eq. (1) with split-step beam propagation method. And the output profiles at z =100 (where the photonic lattice and corresponding BZ turned 30°) are shown in the right panels of Figs. 2(b)−(e), where the right insets depict the output spatial spectra. Most evolution results (except that of point M_2) accord with the profiles of the corresponding Bloch modes with a rotating angle of about 30°. The conclusion can be clearly seen from the output spectra in the momentum space. For instance, the spatial spectrum of Fig. 2(b), which is derived from the Bloch modes of point X_1, is distributed into two bright spots at the two X-points of the rotated BZ. More importantly, due to the Coriolis forces that resist the rotation of the lattice, the two bright spots tend to shift to the opposite direction to the rotation of the lattice. It should be specially noted that the excitation of the Bloch modes at point M_2 is hardly distinguishable, and additional modes are

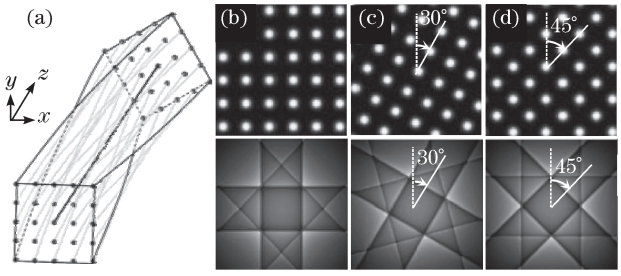

Fig. 1. (a) Geometric schematic of the rotating lattice; (b) BZS of stationary lattice; (c) and (d) BZSs of rotating lattice at z=100 and 150, respectively.

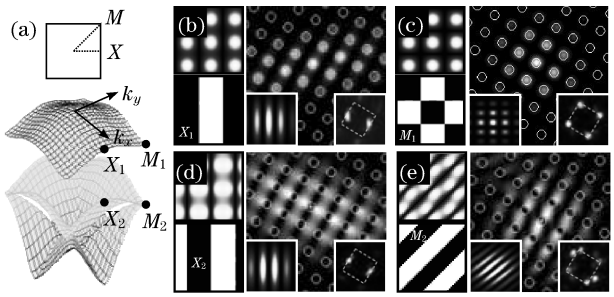

Fig. 2. (a) Band-gap structure of the photonic lattice; (b)−(e) Bloch waves (left) and their propagations in the rotating lattice (right) of points X_1, M_1, X_2, and M_2, respectively. Left insets: input profiles; right insets: spectra of the output fields.

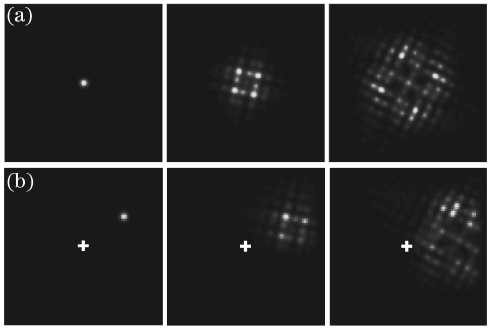

Fig. 3. Discrete diffractions in rotating photonic lattices with incident sites at (a) the central site (0,0) and (b) (20,15); from left to right, they correspond to z=0, 50, and 100, respectively. The crosses denote the central site of the lattices.

excited (Fig. 2(e)). The Bloch wave at point M_2 changes its shape easily in the non-uniform lattices or even in the anisotropic lattices. As a result, under the actions of the changeable Bragg reflections and the Coriolis forces in the rotating lattice, the M_2-point Bloch wave hardly maintained its shape and evolved into mixed modes, as shown in Fig. 2(e). However, the rotating Bragg reflections are still revealed to be supported by the Bloch waves on the whole.

Next, we analyzed the propagations of lattice solitons, which were derived from the balance between discrete diffraction and nonlinearity. First, the linear scheme was explored to study the properties of discrete diffractions in the rotating lattice. To simulate the propagation, a Gaussian probe beam $B_0=0.5\exp[-(x/2.5)^2-(y/2.5)^2]$ was launched into positions (0,0) and (20,15) of the rotating lattice (with lattice space d=5, and (0,0) denoteing the central site), respectively. The results are shown in Fig. 3, illustrating, from left to right, the input beam and output profiles at z=0, 50, and 100, respectively. When launched at the central waveguide (on-axis, see Fig. 3(a)), the discrete diffraction patterns turn around along with the lattice and maintain four-fold symmetry during propagations. When launched at the waveguide away from the center (off-axis, see Fig. 3(b)), the position of the peak intensity remained almost still, owing to Coriolis forces.

To observe the propagation of the discrete solitons, a self-focusing nonlinearity (E_0=1) was added to the rotating lattice. Figure 4 represents the nonlinear prop-

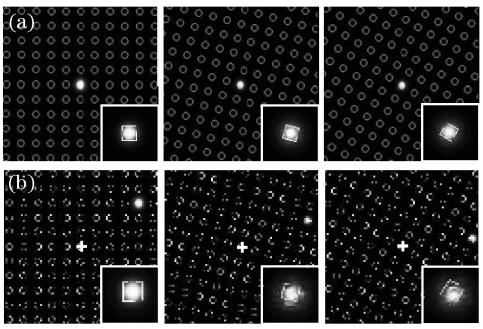

Fig. 4. Discrete solitons in rotating photonic lattices with the incident sites at (a) (0,0) and (b) (20,15); from left to right, they correspond to z=0, 50, and 100, respectively. The insets are the corresponding spatial spectra.

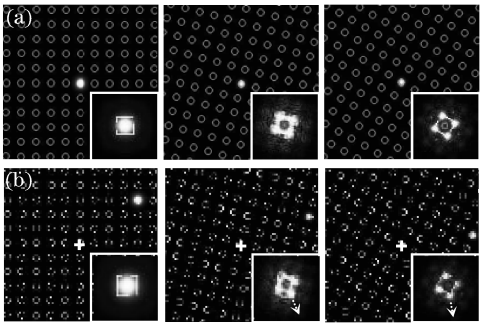

Fig. 5. Gap solitons bifurcating from point M_1 in rotating photonic lattices with the incident sites at (a) (0,0) and (b) (20,15); from left to right, they correspond to z=0, 50, and 100, respectively. The insets are the corresponding spatial spectra.

agations of the probe beam depicted in Fig. 3, which have been launched at positions (0,0) and (20,15) as shown in Figs. 4(a) and (b), respectively. The frames, from left to right, correspond to the respective probe beams and output profiles at z=0, 50, and 100. From the propagation results, the discrete solitons are shown to stably exist in the rotating lattices, no matter whether they are on-axis or off-axis. The soliton stability of the on-axis propagations is due to the lack of external force. Interestingly, the stability of the off-axis discrete soliton has not been ruined, although there is a Coriolis force. Moreover, in the virtue of rotating lattice, an additional angular momentum is added to the discrete soliton, which can be seen from the deviated spots of the spectrum patterns in the insets of Fig. 4(b).

The spreading of the probe beam is enhanced by the presence of self-defocusing nonlinearity. The spatial spectrum of the probe beam is reshaped[13], reaches the boundary of the BZ, and then suffers from the Bragg reflection. Under this condition, gap soliton bifurcating from point M_1 may be formed. To support large gaps, the lattice potential was increased to V_0 =4. Moreover, self-defocusing nonlinearity was introduced by changing the external bias field to E_0 =−4. The simulation results shown in Fig. 5 reveal that, after reshaping the nonlinear spectrum, the probe beams gradually evolve into gap solitons that rotate together with the lattice.

Compared with the on-axis propagation, the off-axis gap soliton obtains an additional angular momentum by the agency of the rotating lattice. The spatial spectrum is not distributed at the four corners of the BZ exactly, but wholly shifts along the direction of instantaneous linear velocity of the soliton (insets of Fig. 5(b)). Furthermore, the gap solitons−whether launched on-axis or off-axis−can steadily propagate for a rather long distance because of the rotating Bragg reflection.

Finally, the gap solitons bifurcating from point X_2 were also investigated. These solitons, called reduced-symmetry solitons, are based on the combined effects of the total internal reflection and Bragg reflection, and represent highly anisotropic symmetry[12]. In the rotating lattice (V_0=2) with a self-focusing nonlinearity (E_0=1), the input beam was modulated as B_0=0.8exp[$-(x/10)^2-(y/5)^2$]sin($\pi x/5$) to match the profile of the Bloch wave at point X_2. Figures 6(a) and (b) depict on-axis and off-axis (launched at (−10,10)) evolutions of the reduced symmetry solitons, respectively. When propagating on-axis, the soliton basically keeps a rotating profile for a long distance. However, due to the anisotropic profile, the soliton suffers the influence of Coriolis forces and presents delayed rotation (see the right side of Fig. 6(a)). When propagating off-axis, the soliton exhibits enhanced mobility. This phenomenon has been previously presented in Ref. [12]. Furthermore, by the action of Coriolis forces, the soliton tends to rotate counterclockwise, in contrast with the lattice. However, due to the reduced symmetry, the soliton moves along the direction where it suffers Bragg reflection (see the arrowhead in Fig. 6(b)), and is trapped in the orthogonal direction. Worth noting is the fact that this type of soliton is unsteady and easily collapses when traveling for a long distance. To restrain the anisotropic symmetry of this soliton, the multi-vortex mode generated by the superposition of two degenerate modes at point X_2 was launched on-axis in the rotating lattice[23]. The evolution is shown in Fig. 6(c), from which a more stable self-trapping state is formed.

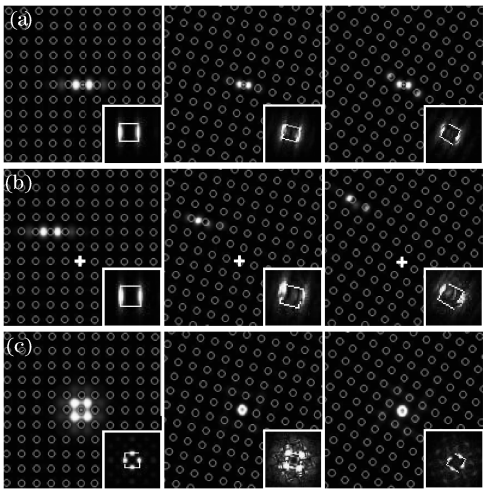

Fig. 6. Propagation of reduced-symmetry solitons (a) on-axis and (b) off-axis (launched at (−10,10)), and (c) multi-vortex solitons bifurcating from point X_2 in rotating photonic lattices. From left to right, they correspond to z=0, 50, and 100, respectively. The insets are the corresponding spatial spectra.

In conclusion, the rotating properties of the Bragg reflection and spatial lattice solitons are demonstrated in the rotating photonic lattices by numerically analyzing the linear and nonlinear light propagations. The Bragg reflections of the rotating lattice, visualized by numerical BZ spectroscopy, are found to rotate following the potential of lattices. The Bloch modes at high symmetric points are simulated by matching the probe beams with the corresponding Bloch waves. Under the influences of the rotating Bragg reflection, the Bloch waves turn around along with the lattices during propagation. In the nonlinear case, the multi-band spatial lattice solitons propagating on-axis and off-axis are excited in the rotating lattices. In the case of off-axis propagation, additional angular momenta are added to the solitons. Interestingly, reduced-symmetry solitons at point X_2 do not easily rotate synchronously with the lattice because of the anisotropic symmetry, which represents enhanced mobility in the modulated direction. However, a stable state can be excited by the multi-vortex modes superposed from the two degenerate modes at point X_2.

This work was supported by the Northwestern Polytechnical University Foundation for Fundamental Research (No. JC200950) and the Doctorate Foundation of Northwestern Polytechnical University (No. CX200914).

References

1. D. N. Christodoulides, F. Lederer, and Y. Silberberg, Nature **424,** 817 (2003).
2. K. Zhou, Z. Guo, and S. Liu, Chin. Opt. Lett. **8,** 791 (2010).
3. S. Liu, P. Zhang, X. Gan, F. Xiao, and J. Zhao, Appl. Phys. B **99,** 727 (2010).
4. T. Pertsch, T. Zentgraf, U. Peschel, A. Bräer, and F. Lederer, Phys. Rev. Lett. **88,** 093901 (2002).
5. C. R. Rosberg, D. N. Neshev, A. A. Sukhorukov, Y. S. Kivshar, and W. Krolikowski, Opt. Lett. **30,** 2293 (2005).
6. P. Zhang, C. Lou, S. Liu, J. Zhao, J. Xu, and Z. Chen, Opt. Lett. **35,** 892 (2010).
7. D. Träger, R. Fischer, D. N. Neshev, A. A. Sukhorukov, C. Denz, W. Królikowski, and Y. S. Kivshar, Opt. Express **14,** 1913 (2006).
8. D. Mandelik, H. S. Eisenberg, and Y. Silberberg, Phy. Rev. Lett. **90,** 053902 (2003).
9. A. A. Sukhorukov, D. Neshev, W. Krolikowski, and Y. S. Kivshar, Phy. Rev. Lett. **92,** 093901 (2004).
10. D. N. Christodoulides and R. I. Joseph, Opt. Lett. **13,** 794 (1988).
11. J. W. Fleischer, M. Segev, N. K. Efremidis, and D. N. Christodoulides, Nature **422,** 147 (2003).
12. R. Fischer, D. Träger, D. N. Neshev, A. A. Sukhorukov, W. Królikowski, C. Denz, and Y. S. Kivshar, Phys. Rev. Lett. **96,** 023905 (2006).
13. C. Lou, X. Wang, J. Xu, and Z. Chen, Phys. Rev. Lett. **98,** 213903 (2007).
14. P. Zhang, S. Liu, J. Zhao, C. Lou, J. Xu, and Z. Chen, Opt. Lett. **33,** 878 (2008).
15. B. Lü, T. Gong, M. Chen, M. Wang, T. Li, G. Chen, and S. Jian, Chin. Opt. Lett. **7,** 656 (2009).
16. V. I. Kopp and A. Z. Genack, Opt. Lett. **28,** 1876 (2003).
17. M. Ornigotti, G. D. Valle, D. Gatti, and S. Longhi, Phys. Rev. A **76,** 023833 (2007).
18. S. Jia and J. W. Fleischer, Phys. Rev. A **79,** 041804 (2009).
19. J. Cuevas, B. A. Malomed, and P. G. Kevrekidis, Phys. Rev. E **76,** 046608 (2007).
20. Y. V. Kartashov, B. A. Malomed, and L. Torner, Phys. Rev. A **75,** 061602(R) (2007).
21. I. L. Garanovich, A. Szameit, A. A. Sukhorukov, T. Pertsch, W. Krolikowski, S. Nolte, D. Neshev, A. Tuennermann, and Y. S. Kivshar, Opt. Express **15,** 9737 (2007).
22. A. A. Zozulya and D. Z. Anderson, Phys. Rev. A **51,** 1520 (1995).
23. S. Liu, P. Zhang, F. Xiao, X. Gan, and J. Zhao, Acta Phys. Sin. (in Chinese) **58,** 5467 (2009).